Cation Dynamics in Mixed-Cation $(MA)_x(FA)_{1-x}PbI_3$ Hybrid Perovskites from Solid-State NMR

Dominik J. Kubicki,[a] Daniel Prochowicz,[b,c] Albert Hofstetter,[a] Péter Péchy,[b] Shaik M. Zakeeruddin,[b] Michael Grätzel,*[b] Lyndon Emsley*[a]

[a]*Laboratory of Magnetic Resonance, Institute of Chemical Sciences and Engineering, Ecole Polytechnique Fédérale de Lausanne (EPFL), CH-1015 Lausanne, Switzerland*
[b]*Laboratory of Photonics and Interfaces, Institute of Chemical Sciences and Engineering, Ecole Polytechnique Fédérale de Lausanne (EPFL), CH-1015 Lausanne, Switzerland*
[c]*Institute of Physical Chemistry, Polish Academy of Sciences, Kasprzaka 44/52, 01-224 Warsaw, Poland.*

Supporting Information Placeholder

ABSTRACT: Mixed cation organic lead halide perovskites attract unfaltering attention owing to their excellent photovoltaic properties. Currently, the best performing perovskite materials contains multiple cations and provide power conversion efficiencies up to around 22%. Here, we report the first quantitative, cation-specific data on cation reorientation dynamics in hybrid mixed-cation formamidinium (FA)/methylammonium (MA) lead halide perovskites. We use ^{14}N, ^{2}H, ^{13}C and ^{1}H solid-state MAS NMR to elucidate cation reorientation dynamics, microscopic phase composition, and the MA/FA ratio, in $(MA)_x(FA)_{1-x}PbI_3$ between 100 and 330 K. The reorientation rates correlate in a striking manner with the carrier lifetimes previously reported for these materials and provide evidence of the polaronic nature of charge carriers in PV perovskites.

INTRODUCTION

Methylammonium ($CH_3NH_3^+$, MA) and formamidinium ($CH(NH_2)_2^+$, FA) cations are two key components of ABX_3 mixed cation metal halide perovskites, which provide an alternative to silicon-based solar cells, with currently achievable power conversion efficiencies up to around 22 %.[1] The single-charged cationic A site is typically formed by MA, FA or Cs^+ enclosed in a perovskite cage formed by $[BX_3]^-$ octahedra (in which $B=Pb^{2+}$, Sn^{2+}, Ge^{2+}, $X=I^-$, Br^-, Cl^-). The systems that are currently providing best power conversion efficiencies and exhibit most favorable current-voltage characteristics and carrier mobility are based on mixed-cation iodoplumbates.[2-3]

Charge carrier lifetimes depend on the perovskite composition, with the mixed cation materials providing longest lifetimes, but so far there is no clear explanation of the mechanism responsible for these differences. Very recently, Gong *et al.*[4] related a difference in carrier lifetimes to a difference in inertia between protonated and deuterated $MAPbI_3$, as measured through time-resolved photoluminescence.

Indeed, a considerable number of experimental methods have been applied to characterize the dynamics of MA in $MAPbX_3$, such as NMR,[5-10], neutron powder diffraction,[11] quasielastic neutron scattering[12] and ultrafast 2DIR vibrational spectroscopy[13-14] as well as theoretical research.[15] This has established that MA is mobile and orientationally disordered at ambient temperature pertinent to the operation of photovoltaic (PC) devices. In particular, it has been shown that the MA cation is not just a passive component only acting as a charge compensation for the $[PbI_3]^-$ lattice; rather, it is actively involved in carrier stabilization by taking on an orientation in which the positive charge interacts with the photogenerated electron in the conduction band formed mainly by the Pb 6p orbitals.[4] The cation reorientation therefore effectively modifies the band structure of the material.[4, 15]

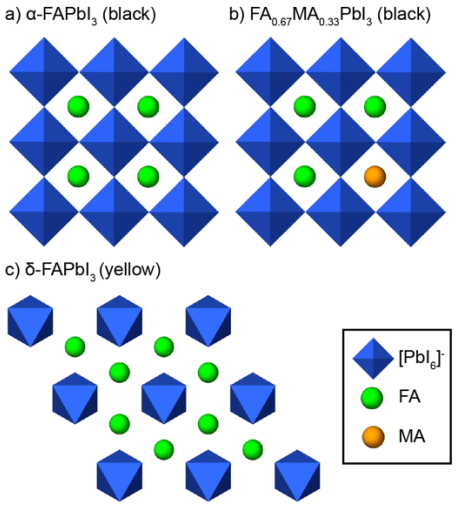

Figure 1. Schematic representation of a) black α-$FAPbI_3$, b) black $(MA)_x(FA)_{1-x}PbI_3$ and c) yellow non-perovskite δ-$FAPbI_3$.

In comparison to $MAPbI_3$, the black cubic perovskite phase α-$FAPbI_3$ (Figure 1a) has advantageous photovoltaic properties as its bandgap (1.40 eV) is closer to the Shockley–Queisser limit of 1.34 eV (1.51 eV in $MAPbI_3$).[16] Relatively little is known about FA dynamics in α-$FAPbI_3$. Molecular dynamics simulations suggested a time constant of 2 ps for the reorientation process at 300 K.[16] However, the pure α-$FAPbI_3$ phase suffers from being thermodynamically unstable at room temperature whereby it undergoes a phase transition to a non-perovskite yellow δ-$FAPbI_3$ phase (Figure 1c). Recently, mixed-organic-cation hybrid perovskites $(MA)_x(FA)_{1-x}PbI_3$ (Figure 1b) have been found to be thermodynamically stable at room temperature, while retaining the excellent properties of the pure FA material.[17] *Ab*

initio calculations link this enhanced stability of mixed phases to their higher entropy and a lower enthalpy of formation than the mixed δ-$FAPbI_3$ phase.[18]

Here, we show that FA reorientation in FA containing materials is faster than MA in the MA material, despite the fact that FA is much larger than MA. The longer carrier lifetimes in the mixed cation materials are thus attributed to faster cation reorientation. More specifically, we show how ^2H and ^{14}N MAS NMR can be used to probe the dynamics of FA and MA separately in mixed-cation $(MA)_x(FA)_{1-x}PbI_3$ perovskites and that their individual dynamics differs significantly from the dynamics of FA and MA in the pure $FAPbI_3$ and $MAPbI_3$ phases. Additionally, we use low-temperature ^{13}C CP MAS NMR to detect with excellent sensitivity the presence of the yellow δ-$FAPbI_3$ and the black α-$FAPbI_3$ phases in $(MA)_x(FA)_{1-x}PbI_3$. We also show that high-resolution ^1H MAS NMR can be used to quantify the FA/MA ratio in the solid powders.

Solid-state NMR has emerged as a particularly useful tool for studying microscopic disorder and phase segregation in $MAPbX_3$ systems. For example, ^{207}Pb NMR chemical shifts have been shown to be very sensitive to the nature of the halogen ions in pure and mixed-halogen hybrid perovskites.[7, 9, 19]. Static ^2H and ^{14}N NMR spectra were used to study the tetragonal-to-cubic transition in $MAPbX_3$ (X=Cl, Br and I)[5, 8] However, both these nuclei have certain limitations associated with them (Table S1). ^2H is a sensitive probe of molecular dynamics in the range of 10^2-10^8 s^{-1} but requires isotopic enrichment which might modify the original cation dynamics. Indeed, MA deuteration has been shown to significantly affect carrier lifetimes in $MAPbI_3$ single crystals and thin films through the recently discovered electron-rotor interaction.[4]

To the best of our knowledge there have been no spectroscopic studies of cation dynamics in mixed-cation $(MA)_x(FA)_{1-x}PbI_3$ hybrid perovskites

Surprisingly, little attention has been given to ^{13}C NMR, which should be a sensitive probe of the local environment and dynamics of the cations. The usual experimental approach assumes the use of cross-polarization (CP)[20] from protons to enhance the ^{13}C sensitivity and reduce recycle delays (which in a CP experiment is dictated by ^1H relaxation, typically much faster than that of ^{13}C). Since the CP transfer relies on H↔C dipole-dipole couplings, which are averaged to zero by isotropic molecular motion, it is not surprising that previously reported CP spectra of $MAPbX_3$ had very low signal-to-noise ratios even after a dozen hours of signal averaging. Direct ^{13}C detection is an alternative which offers little benefit on account of the much slower ^{13}C relaxation.[19] Here we show that the use of low temperatures, where dynamics is significantly reduced, allows access to high sensitivity ^{13}C CPMAS spectra that allow direct determination of the phase composition.

EXPERIMENTAL

Perovskite synthesis and sample preparation. $FA_{0.67}MA_{0.33}PbI_3$ was prepared according to the procedure reported previously.[17] Deuterated $FA(d_4)_{0.67}MA(d_3)_{0.33}PbI_3$ was synthesized using the same procedure but using N-deuterated substrates ($CH_3(ND_2)_2I$ and CH_3ND_3I). N-deuterated FAI and MAI were prepared by proton-deuterium exchange with heavy water (1:40 mole/mole ratio), followed by evaporation.[4] The procedure was repeated 5 times to ensure full deuteration. The substrates ($CH_3(ND_2)_2I$ and CH_3ND_3I) were subsequently dried under vacuum. $FA_{0.90}MA_{0.10}PbI_3$[21], δ-$FAPbI_3$[22] and $MAPbI_3$ were prepared by mechanosynthesis, as described previously.[23] α-$FAPbI_3$ was prepared by heating up δ-$FAPbI_3$ above its phase transition temperature (~125 °C).[24] Perovskite samples were packed into rotors under inert dry nitrogen atmosphere.

NMR measurements. Variable-temperature ^{14}N (32.1 MHz), ^2H (76.8 MHz), ^{13}C (125.7 MHz) and ^1H (500.0 MHz) NMR spectra were recorded on a Bruker Avance III 11.7 T spectrometer equipped with a 3.2 mm low-temperature CPMAS probe. ^1H (800 MHz) MAS experiments were carried out at 18.8 T (Bruker, Avance III) using a standard 1.3 mm CPMAS probe. (Further details in Supplementary Information).

^2H and ^{14}N MAS lineshape analysis. ^{14}N lineshape simulations were carried out using EXPRESS, a MATLAB-based code simulating the effect of dynamics on quadrupolar spectra.[25] Quadrupolar coupling constants were extracted using the SOLA fitting routine incorporated in TopSpin (Bruker).

EFG tensor calculations. The $MAPbI_3$ and $FAPbI_3$ clusters were generated as described in the SI. The EFG tensor calculations were performed at DFT level using the GGA BP86[26-27] functional including relativistic effects (with spin-orbit coupling) with the ZORA[28-30] approximation and the Grimme[31] dispersion correction implemented within the Amsterdam Density Functional (ADF)[32-33] suite. Relativistic effects (with spin-orbit coupling) were taken into account at all calculation stages. Further details can be found in the SI.

RESULTS AND DISCUSSION

Our study sets out to compare the phase composition and dynamics of the following materials of photovoltaic relevance: $MAPbI_3$, α-$FAPbI_3$ (black), δ-$FAPbI_3$ (yellow) and two mixed-cation perovskite compositions: $FA_{0.90}MA_{0.10}PbI_3$, $FA_{0.67}MA_{0.33}PbI_3$ (with the latter two being reported to have excellent PC characteristics[17]) and its N-deuterated variant $FA(d_4)_{0.67}MA(d_3)_{0.33}PbI_3$.

Phase composition from low-temperature ^{13}C CPMAS

While room temperature ^{13}C CPMAS experiments are very insensitive, we find that the CP efficiency in $APbI_3$ perovskites depends quite dramatically on temperature. At temperatures around 100 K CP sensitivity increases dramatically, and it is simple to obtain a good quality spectrum with high signal to noise ratios. This is attributed to significant restriction of the rotational dynamics of the A groups in the perovskite cages. Furthermore, the chemical shifts vary significantly with temperature (spectra at 100 K and 200 K are compared in Figure S1), Thus, signals from the black and yellow phases overlap at 200 K, but they are well resolved at 100 K, allowing straightforward identification of the phase composition at 100 K.

Figure 2a-e shows ^{13}C CP MAS spectra of the series of bulk materials acquired at 100±3 K. The region between 150 and 160 ppm can be ascribed to FA, and between 28 and 34 ppm to MA in different local environments. Of practical importance is the clear-cut difference between the yellow and black $FAPbI_3$ phase. It offers an attractive alternative to powder X-ray diffraction (pXRD), in which the presence or absence of the yellow δ-$FAPbI_3$ phase is concluded based upon its weak low-angle (10.8° 2θ) main reflection that can be obscured altogether in poorly prepared samples.

Previous reports have explored different $FA_xMA_{1-x}PbI_3$ stoichiometries with the overall conclusion that at least 10% of MA is required to stabilize the black $FAPbI_3$ phase under ambient conditions.[17, 34] Inspection of the FA region in Figure 2d and 2e reveals that $FA_{0.90}MA_{0.10}PbI_3$ still contains a considerable amount of the yellow $FAPbI_3$ phase, while $FA_{0.67}MA_{0.33}PbI_3$ is entirely composed of the black phase.

Moving on to the MA region one sees compelling evidence of the MA and FA phases being intimately mixed on the microscopic scale. If the double-cation mixed phases were even to some extent only a physical mixture of the black $FAPbI_3$ and

$MAPbI_3$ phases one would expect to see a peak at 31 ppm in the mixed phase corresponding to pure $MAPbI_3$. Rather, there are two peaks which coalesce at higher temperature (Figure S1) indicating that they both originate from MA cations interacting with FA cations in the neighboring cages. If we exclude the possibility of MA hopping between cages, then the two peaks must correspond to two distinct but different MA environments at low temperature, which coalesce at high temperature once rotational motion sets in. We note that this behavior has so far prevented structure determination at low temperature by single crystal X-ray diffraction.[24] The same consideration applies to the slightly asymmetric shape of the peak for the black FA component which also becomes narrower at higher temperature, consistent with an increase of symmetry. More detailed interpretation using computational methods to predict chemical shifts could shed more light on this low-temperature behavior in the future, but require the use of large unit cells with many heavy atoms.

Intensities of ^{13}C CPMAS spectra are not straightforward to quantify, but the relative amount of FA and MA can be determined with proton NMR. (Liquid-state ^1H NMR has been previously used to quantify the composition of mixed-cation phases after dissolution of the perovskite[35]). Figure 2f shows a ^1H MAS spectrum of a powder of $FA_{0.67}MA_{0.33}PbI_3$ obtained at 800 MHz with fast (40 kHz) MAS. It provides extremely well resolved peaks (FWHM between 130 and 250 Hz) which allow quantitation of the individual components. In this case, by peak integration, we find that the actual composition of the material is $FA_{0.62}MA_{0.38}PbI_3$, within 10% of the calculated FA/MA ratio. (In the following we stick to the convention used in the PV community of reporting composition based on the stoichiometry of substrates (MAI, FAI and PbI_2) taken to the synthesis.)

Note that we also find that the proton T_1 is strongly temperature dependent (Figure 3a). This behavior also reflects the increased rate of motion of the cations as temperature increases and as the system goes through phase transitions (indicated for the pure phases by dashed lines in Figure 3a).[24] The lowest-temperature phase transition of the pure phases studied here is the β→γ transition of $FAPbI_3$ which takes place at ~130 K. It is reasonable to assume that at around 100 K any residual librational phonon modes associated with the rotational movement of the $[PbI_3]^-$ octahedra around the three principal axes will condense leading to a largely rigid solid, and only residual methyl and NH_3^+ group rotation around the C-N axis in MA causes relaxation. A similar trend is observed for deuterium relaxation in $FA(d_4)_{0.67}MA(d_3)_{0.33}PbI_3$ in which all exchangeable (N-H) protons were deuterated (Figure S2). Moreover, since the phase transitions are reversible, there is a one-to-one relationship between the low- and room-temperature materials. The cooling-heating cycle can be repeated many times yielding reproducible results.

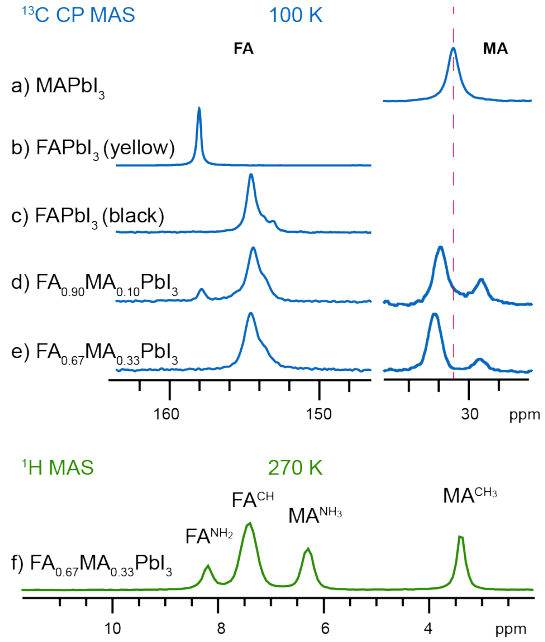

Figure 2. Solid-state MAS NMR spectra of different iodoplumbate phases. ^{13}C CP at 11.7 T and 12 kHz MAS, ^1H at 18.8 T and 40 kHz MAS.

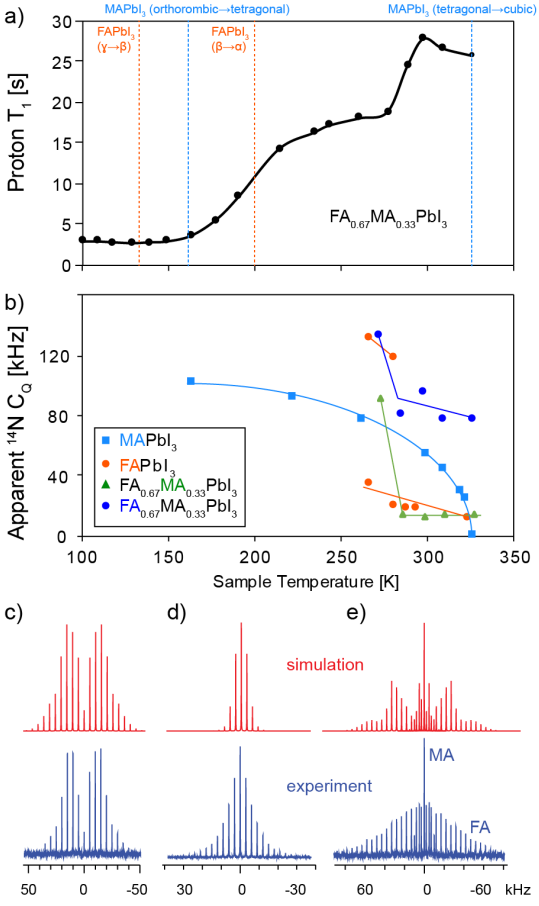

Figure 3. a) Proton T_1 as a function of temperature (12 kHz MAS), measured by fitting ^1H magnetization recovery to a single exponential function. The T_1 reflects an average over all the protons of both FA and MA in the sample of $FA_{0.67}MA_{0.33}PbI_3$. Dotted lines indicate known phase transitions of pure $MAPbI_3$ and $FAPbI_3$ phases for reference. b) Motionally averaged quad-

rupolar coupling constants (C_Q) extracted from ^{14}N variable temperature MAS spectra. Lower C_Q indicates faster reorientation of the EFG tensor (and thus the C–N bond). Solid lines serve as a guide to the eye. Experimental (lower, blue) and simulated (top, red) ^{14}N MAS spectra of c) $MAPbI_3$ (300 K), d) $FAPbI_3$ (294 K) and e) $FA_{0.67}MA_{0.33}PbI_3$ (299 K).

Probing dynamics of individual cations in native double-cation systems

Cation reorientation in perovskites can be probed quantitatively by ^2H and ^{14}N NMR, using well established formalisms.[5, 36]

Variable-temperature ^2H MAS spectra on N-deuterated $FA(d_4)_{0.67}MA(d_3)_{0.33}PbI_3$ are shown in Figure S3. Here the ^2H lineshapes are the result of two processes for both MA and FA: rotation of N-D_3 or N-D_2 groups around the C-N bonds and the overall cation reorientation. It is noteworthy that even below 150 K the apparent C_Q never exceed 80 kHz. This result should be compared with the static C_Q value for methylammonium chloride of 184 kHz.[37] This clearly shows that rotation of the N-D_3 and N-D_2 groups around the C-N bonds is occurring with a correlation time $\tau_c < 10^{-6}$ s even at 100 K (this is in agreement with the T_1 data discussed above). As the temperature increases, we observe the onset of rotational motion of the whole cation which becomes progressively faster leading to a further decrease in apparent C_Q. The apparent ^2H C_Q of MA tends to 0, to within experimental error, above 280 K indicating fast isotropic motion of the N-D bonds,[1] while FA exhibits a small but finite residual ^2H C_Q up to the highest experimentally available temperature here (~330 K), suggesting that the overall motion of the N-D bonds in FA might not be fully isotropic.

Finally, we note that deuteration has been shown to change the intrinsic cation dynamics in lead halide perovskites, such that the ^2H approach above might not be optimal.[4]

The amine nitrogen-14 is a 99.6% abundant spin-1 nucleus characterized, like deuterium, by a non-spherical (quadrupolar) charge distribution, hence it couples to the electric field gradient (EFG, a second-rank tensor) created by the neighboring electrons and nuclei. The magnitude of this quadrupolar coupling, expressed in terms of the nuclear quadrupolar coupling constant C_Q, is typically much larger (1-4 MHz) than for deuterium.[38] Nitrogen-14 spectra of static samples have been previously reported in $MAPbX_3$ model systems.[5, 8] As regards cation dynamics ^{14}N quadrupolar couplings have the advantage that they will not be sensitive to the N-H_3 and N-H_2 motions, and will only be averaged by overall cation mobility.

Figure 4 shows a selection of ^{14}N MAS spectra of $MAPbI_3$, α-$FAPbI_3$ and $FA_{0.67}MA_{0.33}PbI_3$ recorded as a function of temperature. In the single-cation cases only one manifold of spinning sidebands (SSB) is present, whereas in the mixed-cation perovskite two separate manifolds correspond to the two nitrogen-containing species, owing to the difference in their shifts (highlighting the advantage of using MAS here as compared to spectra of static samples). The widths of the spectra decrease with increasing temperature corresponding to a reduction of the averaged quadrupolar coupling constant (Figure 3b). The reorientation of MA in $MAPbI_3$ becomes isotropic with the tetragonal-to-cubic phase transition (326 K, average ^{14}N C_Q=0 kHz, no quadrupolar splitting), in agreement with previous reports.[5, 8]

The average ^{14}N C_Q of FA in $FAPbI_3$ is relatively constant from 330 (the maximum accessible here) to ~280 K, below which temperature a second component with a much larger apparent C_Q appears, corresponding to FA sites with either much slower and/or more restricted motion.

At 327 K, in the mixed $FA_{0.67}MA_{0.33}PbI_3$ perovskite, in contrast to the pure MA phase, the reorientation of the C-N bond in MA at 327 K is not isotropic, as illustrated by the residual lineshape, and for FA it is also different from the pure FA phase ($C_{Q,pure}<C_{Q,mixed}$). This observation provides further proof that in $FA_{0.67}MA_{0.33}PbI_3$ the two cations are intimately mixed (across the whole temperature range studied here), and exhibit properties different to those of the pure phases.

(Note that when the spectra are nearly isotropic under the combined effect of elevated temperature and fast MAS, $^1J_{N\text{-}H}$ couplings become apparent making the signal assignment straightforward (Figure 4, top spectra). The splitting in Figure 4a is not visible due to homogeneous broadening caused by crystal defects, as discussed by Kentgens and coworkers.[8])

Quantitative information on the rate of cation dynamics can be extracted from these ^{14}N MAS spectra by simulating the experimental spectra using a stochastic Liouville formalism.[25] The spectral features generally depend on both the rate and the geometry of motion, but if we assume that the motion is in the regime where the rate is faster than the magnitude of the intrinsic C_Q (the fast motion limit), then the rate can be determined from an analysis of the sideband linewidths.[36] We assume this is the case here at around ambient temperature.

Since at ambient temperature the pure FA phase is cubic and the pure MA phase is close to its second-order tetragonal-to-cubic phase transition, we chose to assume that the reorientation of the cation inside a perovskite cage is well described by a diffusion-in-a-cone model, first developed by Torchia and Szabo[39] and widely used for example to study dynamics in proteins and polymers[40-42]. Numerically this can be approximated as N random jumps between equilibrium positions on the surface of a cone of semiangle θ occurring at rate k (and thus with correlation time $\tau=N^{-1}k^{-1}$). This motion has the effect of partial or full (when θ=54.74°) averaging of the ^{14}N electric field gradient interaction tensor. We found that $N\geq6$ is required to converge to the effect of continuous reorientation (Figure S4) and in what follows we use N=10. The model requires the static quadrupolar coupling constant as an input parameter and to that end we carried out DFT calculations of static ^{14}N EFG tensors in $MAPbI_3$ and $FAPbI_3$ clusters. We found an average static $|C_Q|$=2.81 MHz for the two ^{14}N sites in FA and a static $|C_Q|$=0.77 MHz for the ^{14}N site in MA. The latter value is about 30% higher than that reported by Kentgens *et al*., which was calculated without taking relativistic effects into account.[8] This emphasizes the importance of using relativistic corrections in DFT calculations involving heavy atoms such as lead and iodine. θ is adjusted in order to reproduce the sideband envelope of the experimental spectrum, as shown in figure 3c-e. In all phases except for cubic MA the motion needs to be anisotropic ($\theta\neq$54.74°), an effect which has been predicted by DFT in $MAPbI_3$ and demonstrated experimentally by QENS and ultrafast 2D vibrational spectroscopy.[8, 12-14, 43] We note that the small differences between the simulation and experiment are likely due to the presence of a slight distribution of sites. In all the cases studied, the reorientation takes place in the fast motion limit (FML) and the only effect of increasing reorientation rate k is to narrow linewidths without changing the overall shape of the spectral envelope. This allows us to relate the simulated linewidth (FWHM) to k (Figure S5) and thereby determine k from the experimental

[1] More precisely with cubic or lower symmetry, cubic symmetry being sufficient to average a second rank interaction to zero. In the following we will refer to this as isotropic motion, from the NMR point of view.

FWHM (Table S2). In order to confirm robustness of this approach we checked the effect of θ and the input static quadrupolar coupling constant on the simulated FWHM (Figure S6 and S7, respectively). In the case of FA, an error in the cone semi-angle leading to a 4 times broader spectral envelope translates to only 10% difference in the simulated FWHM, which has a <1% effect of the reorientation time constant.

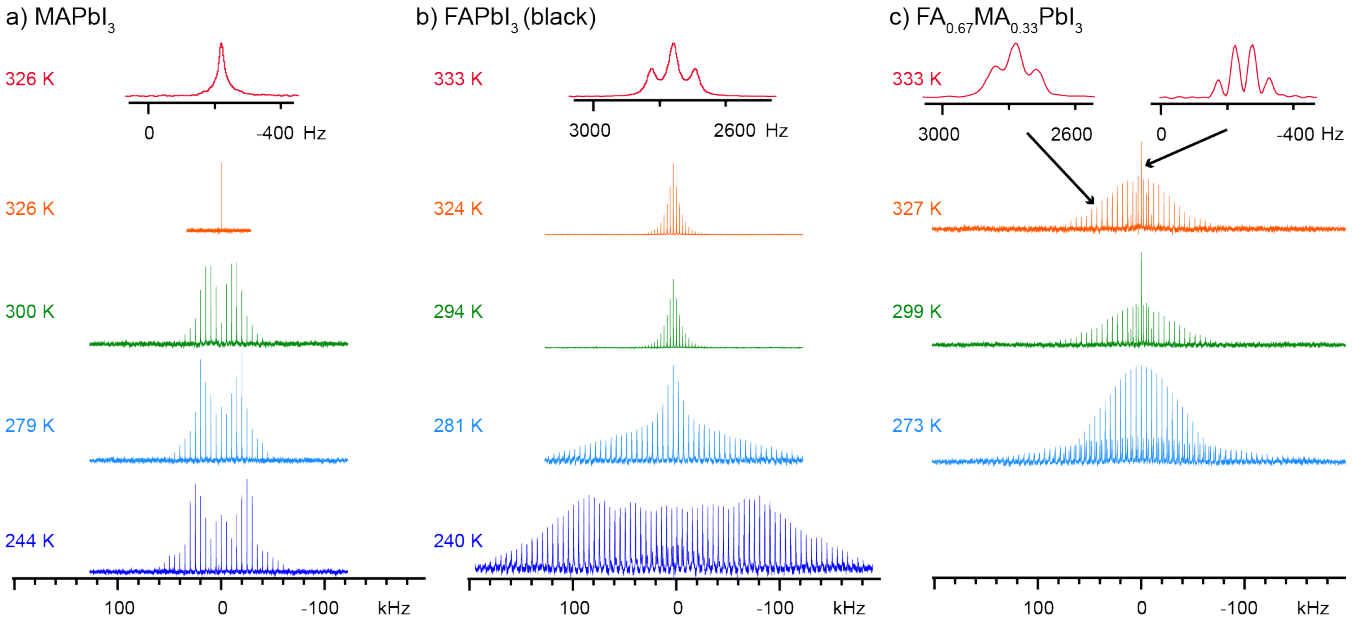

Figure 4. Solid-state ^{14}N echo-detected variable-temperature MAS NMR spectra. The MAS rate was either 3 or 5 kHz (between 240 and 327 K) and 20 kHz for the two top 333 K spectra in b) and c). The top insets (red) show a close-up of the central peak with a characteristic splitting due to the familiar *J*-coupling between the nitrogen and the proton.

The effect of the static C_Q is more significant. Mis-setting by 20% leads to a time constant from shorter by 30% to longer by 60%. We note, however, that given the accuracy of fully-relativistic DFT calculations, the deviation of the static C_Q from the computed values is unlikely to be significant, and certainly not large enough to change the qualitative conclusion of this study (a factor of 4 difference between the static C_Q values of MA and FA leads to ca. 10 times faster reorientation of FA). When, however, the experimental static C_Q values become available, the protocol described here can be easily reapplied to improve accuracy of the reported reorientation correlation times. The largest source of error is thus expected to be the measure of the FWHM, with the errors reported in Table S2 given at 3 standard deviations. The experimental linewidths were obtained as an average from a mixed Gaussian-Lorentzian fit of the most intense sidebands and are summarized in Table S2. The limiting homogeneous broadening is estimated from the temperature dependence of the linewidths.

A comment is in order regarding the underlying physical meaning of the reorientation correlation times obtained from the diffusion-in-a-cone model. Its fundamental feature is that it describes a motion using two parameters (cone semiangle θ and rate k) without invoking the *physical* path the reorienting moiety follows.[39, 44] The model derives its power from this simplicity which rendered it a gold standard to analyze dynamics in solid-state NMR. The situation is different in optical spectroscopies (such as 2DIR) and in neutron scattering experiments, which require a physical model of reorientation in order to analyze data. This renders the two approaches not commensurable and explains the discrepancy between the absolute values of reorientation correlation times in our results (108±18 ps) and those previously reported for $MAPbI_3$ (1-14 ps)[12-14, 43]. That said, the conclusions drawn from the diffusion-in-a-cone model are based on the relative values obtained using the same approach for a series of structures. They are fully valid within the framework of the model we adopted.

Table 1. Cation reorientation correlation times from ^{14}N MAS spectra of $APbI_3$ perovskites.

A	T [K]	τ [ps]
MA	300	108 ± 18
FA	294	8.7 ± 0.5
$FA_{0.67}MA_{0.33}$	299	MA: 133 ± 46 FA: 12 ± 5

The reorientation rates that we determine in this way are given in Table 1 for $MAPbI_3$, $FAPbI_3$ a mixed FA/MA system. We find that FA rotates faster than MA, both in the pure material, and in the mixed perovskites where both MA and FA are simultaneously present and found to be reorienting at different rates. Notably, FA and MA appear to rotate at the same rates (to within error) in both the respective pure phase and in the mixed phase. It may appear counterintuitive that FA reorients faster that MA even though it is bulkier. However, MA is a stronger proton donor than FA and therefore its propensity to form hydrogen bonds with the iodide atoms is expected to be higher, thereby restraining its motion to some extent.

These findings correlate in a striking manner with the charge carrier lifetimes previously reported for these materials, where carrier lifetimes in $FAPbI_3$ and mixed-cation FA/MA lead iodide perovskites were found to be significantly longer than in $MAPbI_3$.[17] As mentioned in the introduction, previous work found that

charge-carrier lifetimes are correlated to the rotational momentum of the rotors, with faster rotation leading to better orbital overlap, easier polaron formation and therefore to the electrons overcoming recombination more efficiently.[4] Further, our finding provides a natural explanation of the fact that charge carrier lifetimes in PV perovskites decrease with temperature, a striking property which stands in stark contrast to classic semiconductors, such as Si or GaAs, in which charge recombination is a phonon-driven process and is thus hampered at lower temperatures.[45-46] More specifically, below 120 K charge carrier lifetimes were observed to drop abruptly, by an order of magnitude, consistent with freezing of the whole-body reorientation of the cation, as determined from ^{2}H spectra in this work. Other work[47] has reported that the fill factor (FF) of a $MAPbI_3$-based cell decreased roughly linearly with temperature, by a factor of 2.6 between 300 and 100 K, and led to a similar trend in the photovoltaic efficiency (PCE) (decrease by a factor of 3 between 300 and 100 K). This effect was tentatively attributed to the activation of trap states and defects. However, it appears likely from our work that the decrease in FF is caused by the accompanying reduction in charge carrier lifetimes due to slowing of cation dynamics.

Finally, our findings provide further evidence of the polaronic nature of charge carriers in PV perovskites.[48-49]

CONCLUSIONS

In summary, we have shown that low-temperature ^{13}C MAS NMR can be used as a quick and sensitive check of phase purity in single and mixed-cation systems. High-field (≥800 MHz) fast MAS ^{1}H spectra can be used for routine quantification of the cation ratio in solid PV materials.

^{2}H and, in particular, ^{14}N MAS provide quantitative information on cation dynamics at ambient temperature. We find that FA rotates faster than MA, both in the pure material, and in the mixed perovskites where both MA and FA are simultaneously present and found to be reorienting at different rates. These findings correlate in a striking manner with measured charge carrier lifetimes, suggesting that the PV properties are correlated directly to cation reorientation and confirming the polaronic nature of charge carriers in PV perovskites. We highlight that NMR is unique in that it allows the two cations to be probed simultaneously in a mixed-cation sample. One obvious conclusion is that if materials can be designed in the future to have faster cation rotation, all other things being equal, then they are likely to have better PV properties.

ASSOCIATED CONTENT

Supporting Information

Complementary NMR data, details of simulations and DFT calculations. Key properties of NMR-active nuclei pertinent to photovoltaic materials.

AUTHOR INFORMATION

Corresponding Authors

*michael.graetzel@epfl.ch
*lyndon.emsley@epfl.ch

Notes

The authors declare no competing financial interests.

ACKNOWLEDGMENT

This work was supported by ERC Advanced Grant No. 320860. D. P. acknowledges support from the co-funded Marie Skłodowska-Curie fellowship, H2020, grant agreement no. 707168.

REFERENCES

1. Saliba, M.; Matsui, T.; Domanski, K.; Seo, J. Y.; Ummadisingu, A.; Zakeeruddin, S. M.; Correa-Baena, J. P.; Tress, W. R.; Abate, A.; Hagfeldt, A.; Gratzel, M., *Science* **2016,** *354* (6309), 206-209.
2. Jeon, N. J.; Noh, J. H.; Yang, W. S.; Kim, Y. C.; Ryu, S.; Seo, J.; Seok, S. I., *Nature* **2015,** *517* (7535), 476-480.
3. Li, X.; Bi, D. Q.; Yi, C. Y.; Decoppet, J. D.; Luo, J. S.; Zakeeruddin, S. M.; Hagfeldt, A.; Gratzel, M., *Science* **2016,** *353* (6294), 58-62.
4. Gong, J.; Yang, M. J.; Ma, X. C.; Schaller, R. D.; Liu, G.; Kong, L. P.; Yang, Y.; Beard, M. C.; Lesslie, M.; Dai, Y.; Huang, B. B.; Zhu, K.; Xu, T., *J. Phys. Chem. Lett.* **2016,** *7* (15), 2879-2887.
5. Knop, O.; Wasylishen, R. E.; White, M. A.; Cameron, T. S.; Vanoort, M. J. M., *Can. J. Chem.* **1990,** *68* (3), 412-422.
6. Baikie, T.; Barrow, N. S.; Fang, Y. A.; Keenan, P. J.; Slater, P. R.; Piltz, R. O.; Gutmann, M.; Mhaisalkar, S. G.; White, T. J., *J. Mater. Chem. A* **2015,** *3* (17), 9298-9307.
7. Rosales, B. A.; Men, L.; Cady, S. D.; Hanrahan, M. P.; Rossini, A. J.; Vela, J., *Chem. Mater.* **2016,** *28* (19), 6848-6859.
8. Franssen, W. M. J.; van Es, S. G. D.; Dervisoglu, R.; de Wijs, G. A.; Kentgens, A. P. M., *J. Phys. Chem. Lett.* **2017,** *8* (1), 61-66.
9. Rosales, B. A.; Hanrahan, M. P.; Boote, B. W.; Rossini, A. J.; Smith, E. A.; Vela, J., *ACS Energy Lett.* **2017,** *2*, 906-914.
10. Senocrate, A.; Moudrakovski, I.; Kim, G.-Y.; Yang, T.-Y.; Gregori, G.; Gratzel, M.; Maier, J., *Angew. Chem. Int. Ed.* **2017,** *56*.
11. Weller, M. T.; Weber, O. J.; Henry, P. F.; Di Pumpo, A. M.; Hansen, T. C., *Chem. Commun.* **2015,** *51* (20), 4180-4183.
12. Leguy, A. M. A.; Frost, J. M.; McMahon, A. P.; Sakai, V. G.; Kochelmann, W.; Law, C. H.; Li, X. E.; Foglia, F.; Walsh, A.; O'Regan, B. C.; Nelson, J.; Cabral, J. T.; Barnes, P. R. F., *Nat. Commun.* **2015,** *6*, 7124-7133.
13. Bakulin, A. A.; Selig, O.; Bakker, H. J.; Rezus, Y. L. A.; Muller, C.; Glaser, T.; Lovrincic, R.; Sun, Z. H.; Chen, Z. Y.; Walsh, A.;

Frost, J. M.; Jansen, T. L. C., *J. Phys. Chem. Lett.* **2015,** *6* (18), 3663-3669.
14. Selig, O.; Sadhanala, A.; Muller, C.; Lovrincic, R.; Chen, Z. Y.; Rezus, Y. L. A.; Frost, J. M.; Jansen, T. L. C.; Bakulin, A. A., *J. Am. Chem. Soc.* **2017**, 4068-4074.
15. Motta, C.; El-Mellouhi, F.; Kais, S.; Tabet, N.; Alharbi, F.; Sanvito, S., *Nat. Commun.* **2015,** *6*, 7026-7032.
16. Weller, M. T.; Weber, O. J.; Frost, J. M.; Walsh, A., *J. Phys. Chem. Lett.* **2015,** *6* (16), 3209-3212.
17. Pellet, N.; Gao, P.; Gregori, G.; Yang, T. Y.; Nazeeruddin, M. K.; Maier, J.; Gratzel, M., *Angew. Chem. Int. Ed. Engl.* **2014,** *53* (12), 3151-3157.
18. Yi, C. Y.; Luo, J. S.; Meloni, S.; Boziki, A.; Ashari-Astani, N.; Gratzel, C.; Zakeeruddin, S. M.; Rothlisberger, U.; Gratzel, M., *Energy Environ. Sci.* **2016,** *9* (2), 656-662.
19. Roiland, C.; Trippe-Allard, G.; Jemli, K.; Alonso, B.; Ameline, J. C.; Gautier, R.; Bataille, T.; Le Polles, L.; Deleporte, E.; Even, J.; Katan, C., *PCCP* **2016,** *18* (39), 27133-27142.
20. Pines, A.; Gibby, M. G.; Waugh, J. S., *J. Chem. Phys.* **1973,** *59* (2), 569-590.
21. Prochowicz, D.; Yadav, P.; Saliba, M.; Saski, S. M.; Zakeeruddin, S. M.; Lewinski, J.; Gratzel, M., *Sustainable Energy and Fuels* **2017**, 689-693.
22. Jodlowski, A. D.; Yepez, A.; Luque, R.; Camacho, L.; de Miguel, G., *Angew. Chem. Int. Ed. Engl.* **2016,** *55* (48), 14972-14977.
23. Prochowicz, D.; Franckevicius, M.; Cieslak, A. M.; Zakeeruddin, S. M.; Gratzel, M.; Lewinski, J., *J. Mater. Chem. A* **2015,** *3* (41), 20772-20777.
24. Stoumpos, C. C.; Malliakas, C. D.; Kanatzidis, M. G., *Inorg. Chem.* **2013,** *52* (15), 9019-9038.
25. Vold, R. L.; Hoatson, G. L., *J. Magn. Reson.* **2009,** *198* (1), 57-72.
26. Perdew, J. P., *Physical Review B* **1986,** *33* (12), 8822-8824.
27. Becke, A. D., *Physical Review A* **1988,** *38* (6), 3098-3100.
28. Vanlenthe, E.; Baerends, E. J.; Snijders, J. G., *J. Chem. Phys.* **1994,** *101* (11), 9783-9792.
29. Vanlenthe, E.; Baerends, E. J.; Snijders, J. G., *J. Chem. Phys.* **1993,** *99* (6), 4597-4610.
30. van Lenthe, E.; Ehlers, A.; Baerends, E. J., *J. Chem. Phys.* **1999,** *110* (18), 8943-8953.
31. Grimme, S., *J. Comput. Chem.* **2006,** *27* (15), 1787-1799.
32. Guerra, C. F.; Snijders, J. G.; te Velde, G.; Baerends, E. J., *Theor. Chem. Acc.* **1998,** *99* (6), 391-403.
33. te Velde, G.; Bickelhaupt, F. M.; Baerends, E. J.; Guerra, C. F.; Van Gisbergen, S. J. A.; Snijders, J. G.; Ziegler, T., *J. Comput. Chem.* **2001,** *22* (9), 931-967.
34. Binek, A.; Hanusch, F. C.; Docampo, P.; Bein, T., *J. Phys. Chem. Lett.* **2015,** *6* (7), 1249-1253.
35. Weber, O. J.; Charles, B.; Weller, M. T., *J. Mater. Chem. A* **2016,** *4* (40), 15375-15382.
36. O'Dell, L. A.; Ratcliffe, C. I., Quadrupolar NMR to Investigate Dynamics in Solid Materials. In *NMR of Quadrupolar Nuclei in Solid Materials*, Wasylishen, R. E.; Ashbrook, S. E.; Wimperis, S., Eds. Wiley: 2011.
37. Hunt, M. J.; Mackay, A. L., *J. Magn. Reson.* **1974,** *15* (3), 402-414.
38. O'Dell, L. A.; Schurko, R. W.; Harris, K. J.; Autschbach, J.; Ratcliffe, C. I., *J. Am. Chem. Soc.* **2011,** *133* (3), 527-546.
39. Torchia, D. A.; Szabo, A., *J. Magn. Reson.* **1982,** *49* (1), 107-121.
40. Giraud, N.; Blackledge, M.; Goldman, M.; Bockmann, A.; Lesage, A.; Penin, F.; Emsley, L., *J. Am. Chem. Soc.* **2005,** *127* (51), 18190-18201.
41. Smith, A. A.; Testori, E.; Cadalbert, R.; Meier, B. H.; Ernst, M., *J. Biomol. NMR* **2016,** *65* (3-4), 171-191.
42. Hansen, M. R.; Graf, R.; Spiess, H. W., *Chem. Rev.* **2016,** *116* (3), 1272-1308.
43. Chen, T.; Foley, B. J.; Ipek, B.; Tyagi, M.; Copley, J. R. D.; Brown, C. M.; Choi, J. J.; Lee, S. H., *PCCP* **2015,** *17* (46), 31278-31286.
44. Lipari, G.; Szabo, A., *J. Am. Chem. Soc.* **1982,** *104* (17), 4546-4559.
45. Wehrenfennig, C.; Liu, M. Z.; Snaith, H. J.; Johnston, M. B.; Herz, L. M., *Apl Materials* **2014,** *2* (8).
46. Sarang, S.; Ishihara, H.; Chen, Y. C.; Lin, O.; Gopinathan, A.; Tung, V. C.; Ghosh, S., *PCCP* **2016,** *18* (41), 28428-28433.
47. Leong, W. L.; Ooi, Z. E.; Sabba, D.; Yi, C. Y.; Zakeeruddin, S. M.; Graetzel, M.; Gordon, J. M.; Katz, E. A.; Mathews, N., *Adv. Mater.* **2016,** *28* (12), 2439-2445.
48. Zhu, X. Y.; Podzorov, V., *J. Phys. Chem. Lett.* **2015,** *6* (23), 4758-4761.
49. Frost, J. M.; Walsh, A., *Acc. Chem. Res.* **2016,** *49* (3), 528-535.

TOC:

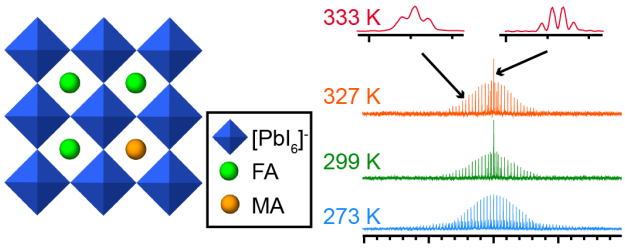

Cation Dynamics in Mixed-Cation $(MA)_x(FA)_{1-x}PbI_3$ Hybrid Perovskites from Solid-State NMR

Dominik J. Kubicki,[a] Daniel Prochowicz,[b] Albert Hofstetter,[a] Péter Péchy,[b] Shaik M. Zakeeruddin,[b] Michael Grätzel,*[b] Lyndon Emsley*[a]

[a]*Laboratory of Magnetic Resonance, Institute of Chemical Sciences and Engineering, Ecole Polytechnique Fédérale de Lausanne (EPFL), CH-1015 Lausanne, Switzerland*
[b]*Laboratory of Photonics and Interfaces, Institute of Chemical Sciences and Engineering, Ecole Polytechnique Fédérale de Lausanne (EPFL), CH-1015 Lausanne, Switzerland*

Table of Contents

Table S1. Key properties of NMR-active nuclei pertinent to photovoltaic materials.

Nucleus	Spin	Nat. abund. [%]	Receptivity rel. to ^{13}C	Characteristics
^{1}H	½	99.99	5870	Excellent sensitivity, easy FA/MA ratio quantitation at ≥800 MHz.
^{2}H	1	0.01	0.0065	Sensitive to phase transitions (through cation dynamics)[1-2], but cation reorientation difficult to probe quantitatively. Requires isotopic enrichment which inherently alters the dynamics compared to the native material.[3]
^{13}C	½	1.07	1	A sensitive indicator of phase composition (e.g. yellow/black $FAPbI_3$), although typically not quantitative. CP MAS provides good sensitivity but only works well in rigid systems (T~100 K).
^{14}N	1	99.63	5.88	Sensitive to cation reorientation dynamics in the native material but practically limited to the fast-motion regime (tetragonal and cubic phases), otherwise the linewidths are prohibitively broad.
^{15}N	½	0.37	0.023	Narrow lines, potentially a sensitive probe of phase composition but requires a costly isotopic enrichment which modifies the sample.
^{207}Pb	½	22.1	22.1	A sensitive probe of the lead-halogen interaction and $[PbX_3]^-$ symmetry[2, 4-5] but comparatively insensitive to the A-site composition (Figure S8)

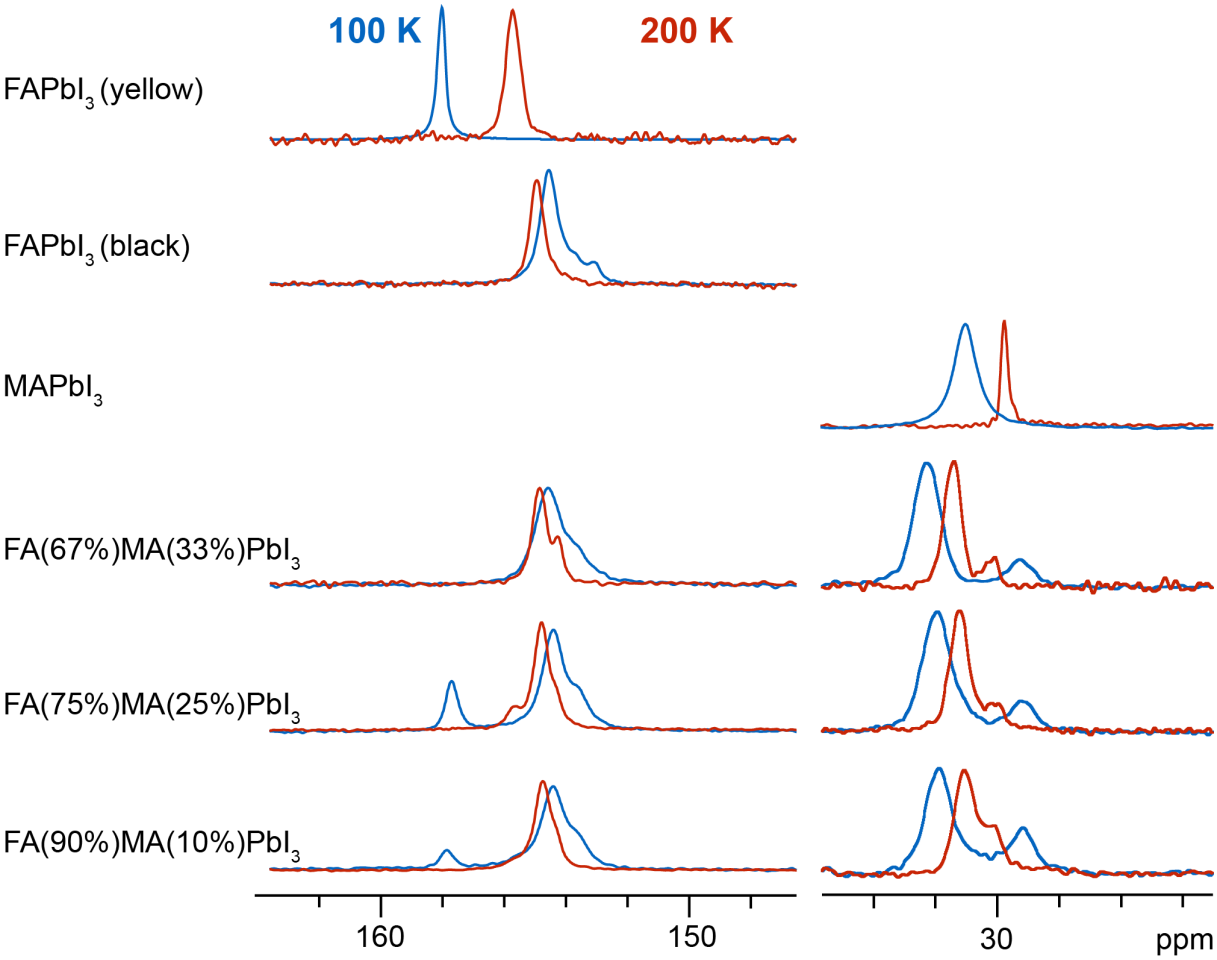

Figure S1. Solid-state ^{13}C CP MAS NMR spectra of different iodoplumbate phases at 9.4 T, 12 kHz MAS and two different temperatures (100 and 200 K).

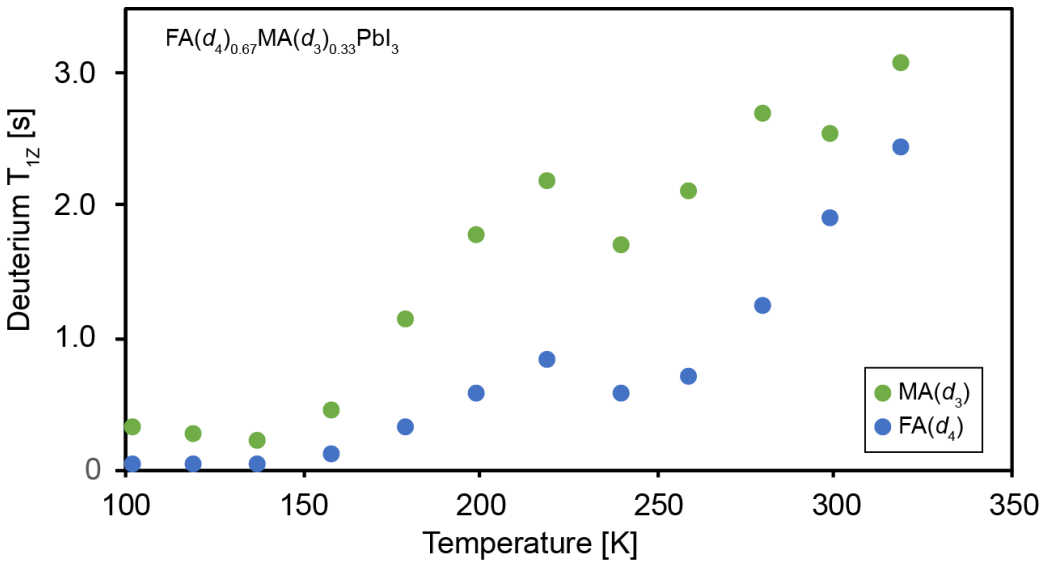

Figure S2. ^{2}H T_{1Z} relaxation in in $FA(d_4)_{0.67}MA(d_3)_{0.33}PbI_3$ as a function of temperature.

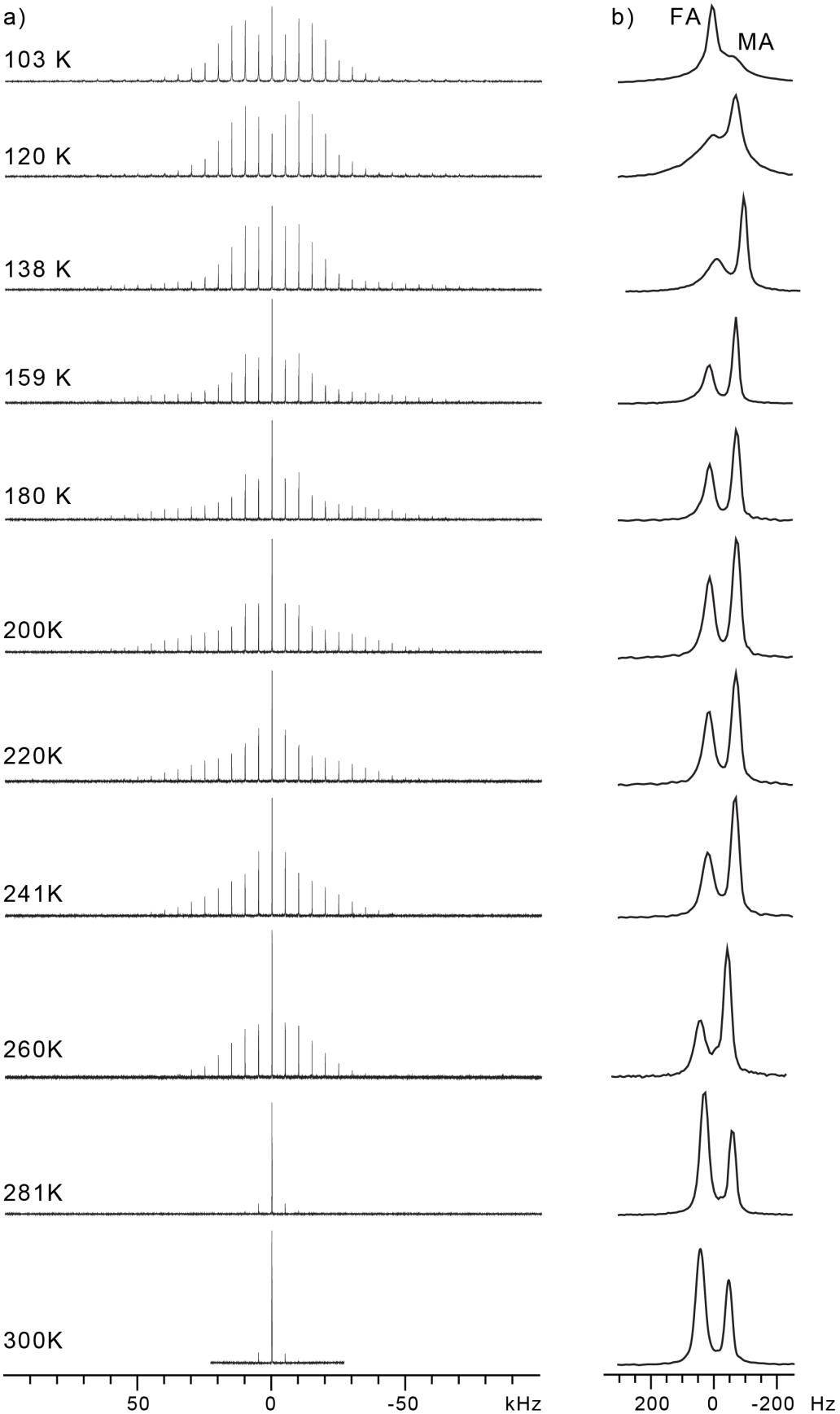

Figure S3. Variable-temperature echo-detected ^{2}H MAS spectra $FA(d_4)_{0.67}MA(d_3)_{0.33}PbI_3$: a) the full spectrum b) a close-up of the central line

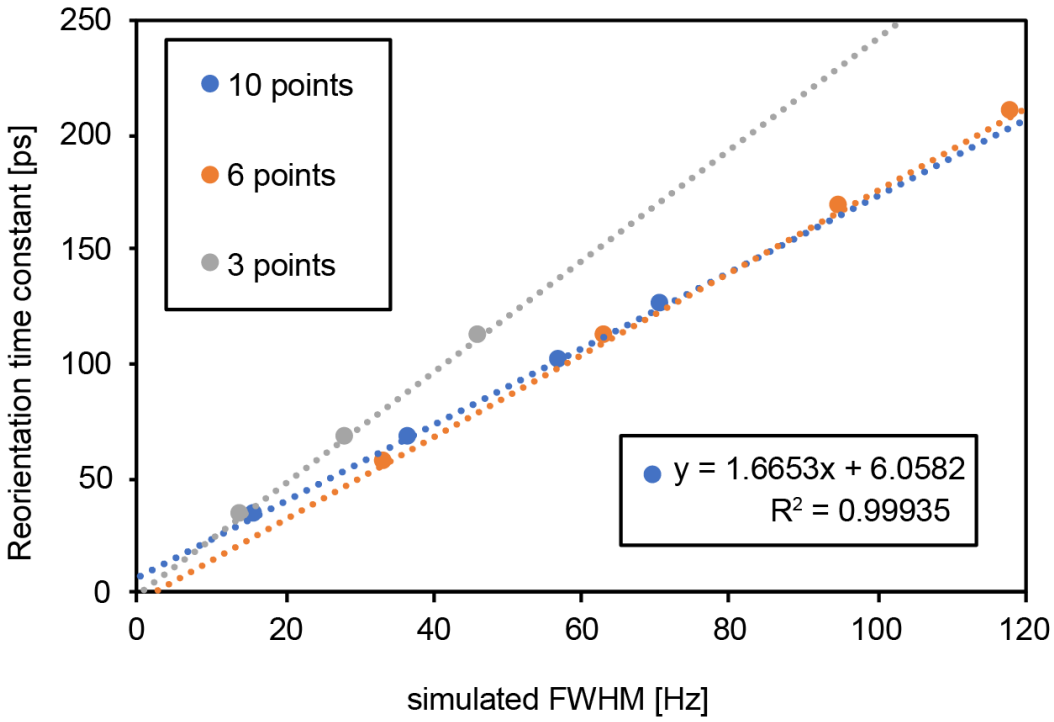

Figure S4. Diffusion-in-a-cone averaging using different number of points and EFG parameters for MA (C_Q=0.771 MHz) and cone semiangle ϑ=51.70°. For further details see the description in the main text.

a)

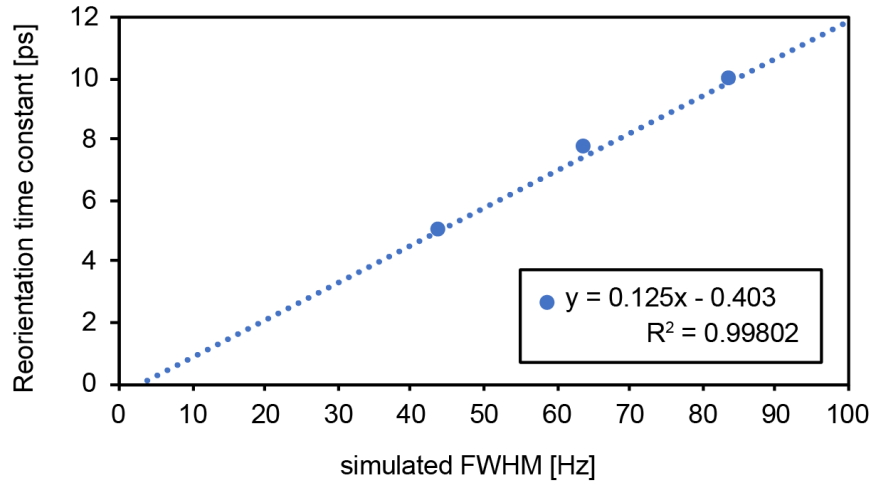

b)

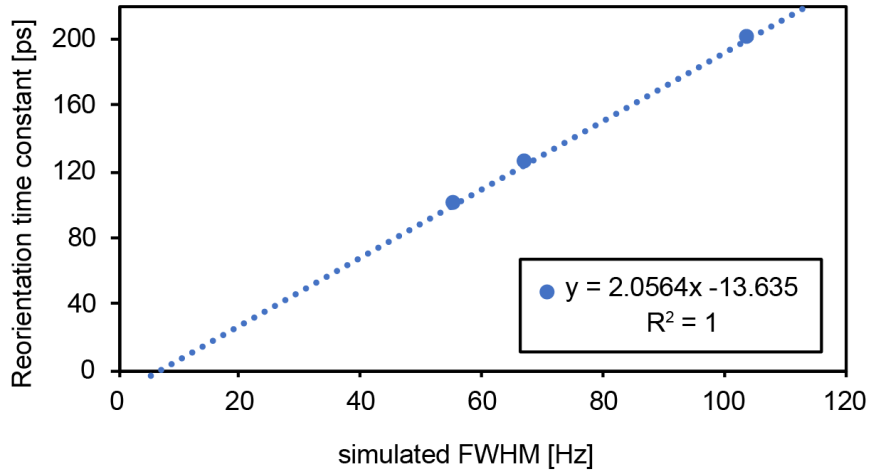

c)

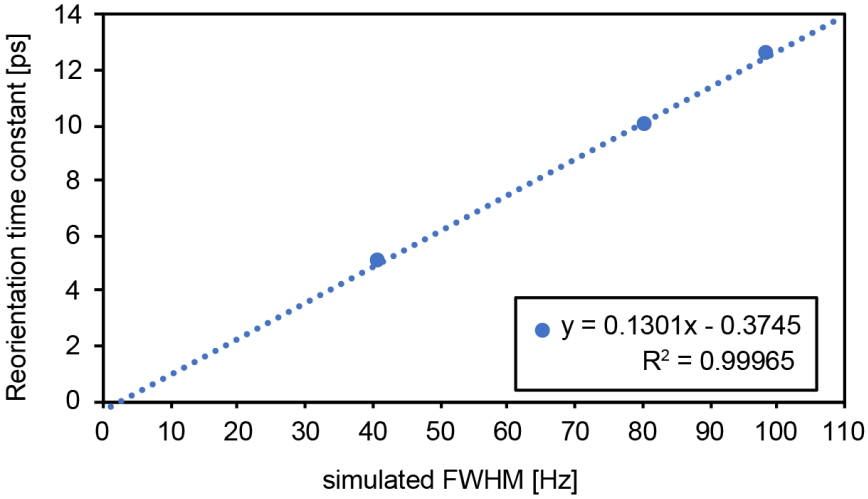

Figure S5. Diffusion-in-a-cone averaging using 10 points on a cone for a) FA in $FAPbI_3$ at 294 K (C_Q=2.810 MHz, ϑ=52.3°); b) MA in $FA_{0.67}MA_{0.33}PbI_3$ at 299 K (C_Q=0.771 MHz, ϑ=53.37°); c) FA in $FA_{0.67}MA_{0.33}PbI_3$ at 299 K (C_Q=2.810 MHz, ϑ=51.6°). For further details see the description in the main text.

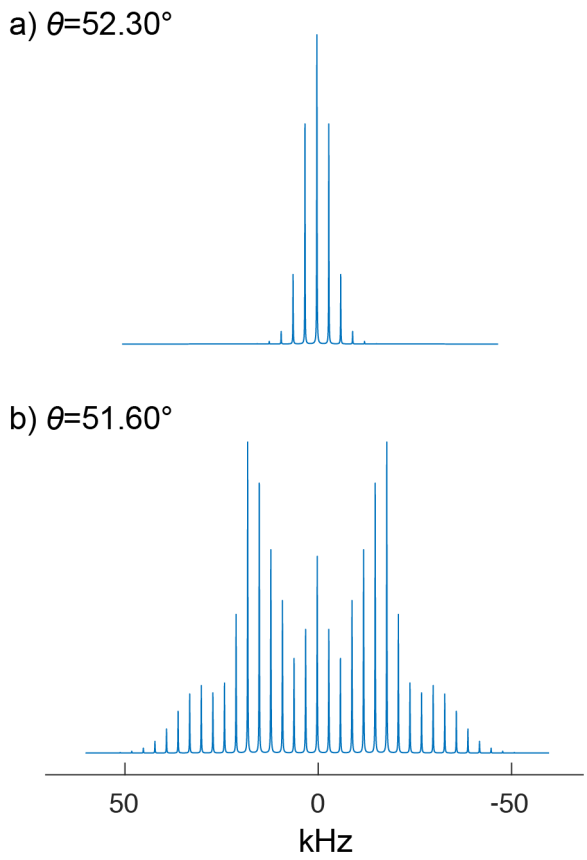

Figure S6. Illustration of the effect of misseting the cone semiangle ϑ (C_Q=2.810 MHz, simulated reorientation time τ=10 ps).

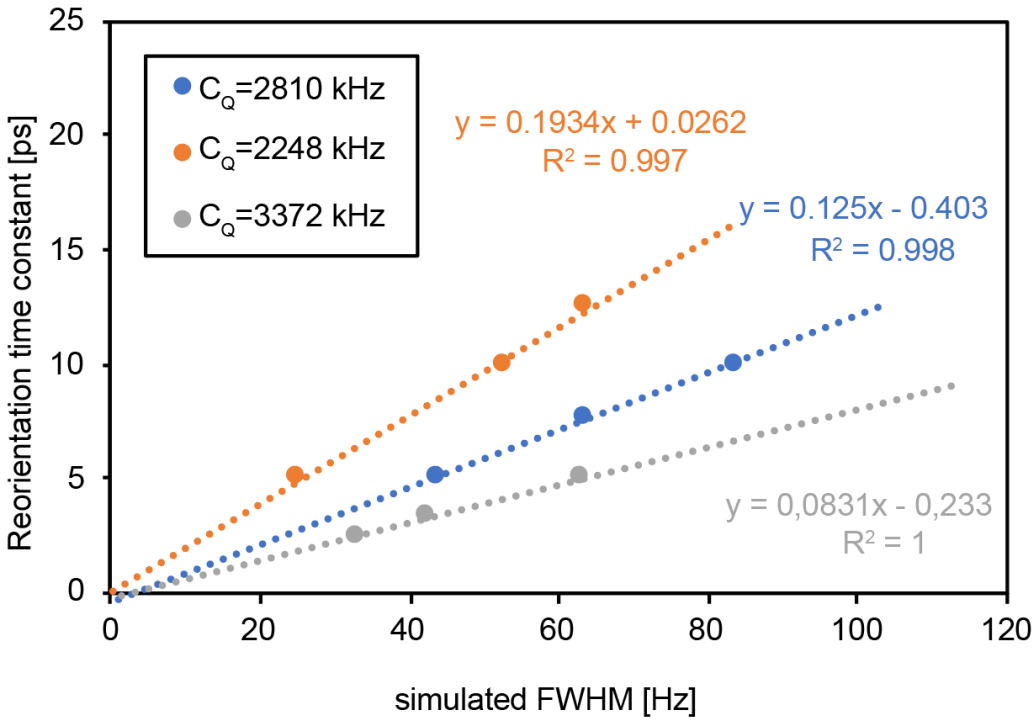

Figure S7. Illustration of the effect of static C_Q on the reorientation correlation time.

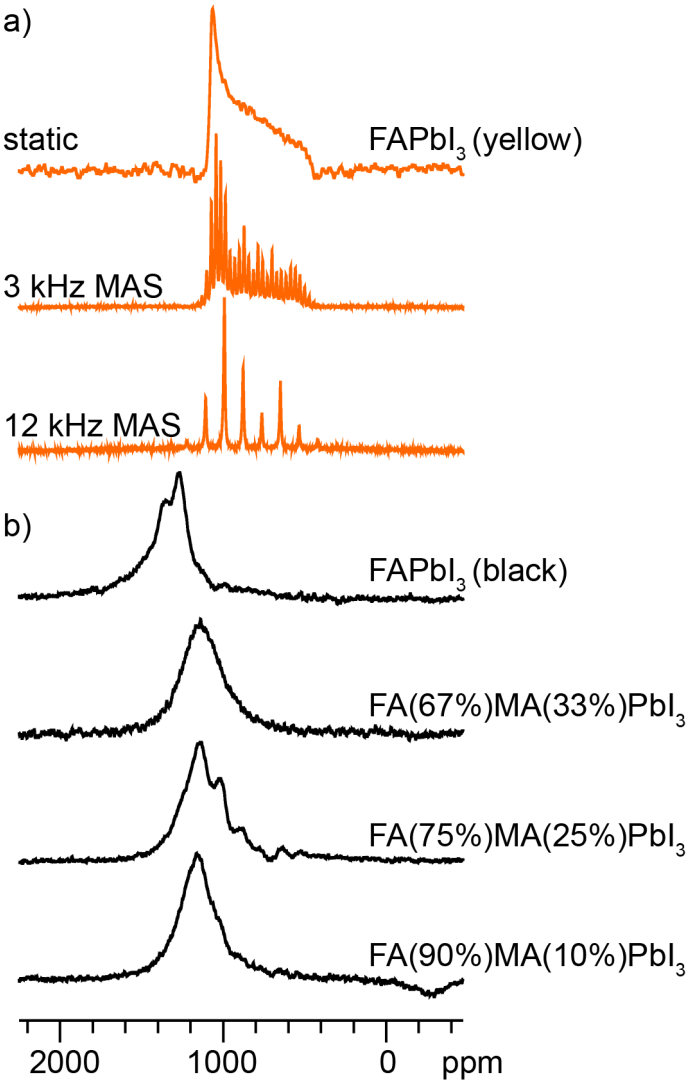

Figure S8. ^{207}Pb echo-detected spectra of different iodoplumbate phases at 11.7 T and 100 K. a) δ-FAPbI3 at two different spinning speeds and static showing the broadening originates from chemical shift anisotropy (CSA). b) Black perovskite phases at 12 kHz MAS. In this case, the broadening is not affected by spinning. Its likely origin is the recently reported fast MAS-induced relaxation due to the crossing of ^{207}Pb and ^{127}I energy levels.[6]

Table S2. Full widths at half maximum (FWHM) and standard deviations (σ) obtained by fitting (SOLA) the most intense peaks (best SNR) in ^{14}N MAS spectra. The standard deviation of the average FWHM is a square root of the average variance (σ^2).

	MAPbI_3 at 300 K, 5 kHz MAS			**FA**PbI_3 at 294 K, 3 kHz MAS			**$FA_{0.67}MA_{0.33}PbI_3$** at 299 K, 5 kHz MAS					
	FWHM [Hz]	σ	σ^2	FWHM [Hz]	σ	σ^2	FWHM (**FA**) [Hz]	σ	σ^2	FWHM (**MA**) [Hz]	σ	σ^2
	60.5	1.8	3.1	80.0	0.8	0.7	96.5	2.3	5.5	66.8	4.6	21.3
	61.5	0.9	0.9	75.1	0.5	0.2	94.2	1.9	3.5	69.8	4.5	20.4
	59.5	0.6	0.3	70.6	0.3	0.1	99.8	1.9	3.8	71.3	2.3	5.2
	61.9	0.6	0.4	68.4	0.2	0.1	95.0	3.4	11.8	76.4	2.9	8.1
	70.7	1.8	3.3	67.5	0.2	0.1	89.3	7.2	51.7			
	60.7	1.0	1.0	69.2	0.2	0.0	94.8	7.7	59.2			
	63.6	0.7	0.5	71.4	0.3	0.1	98.1	3.9	15.0			
	57.5	0.6	0.3	72.5	0.5	0.3	96.6	2.2	4.6			
	59.6	0.8	0.7	79.2	0.7	0.5	85.0	2.3	5.3			
	58.1	1.7	2.9									
avg	**61.4**	3.6	13.3	**72.7**	1.4	2.0	**94.4**	12.7	160.4	**71.1**	7.4	55.0

Table S3. Temperature dependence of FWHM in ^{14}N spectra of perovskites. The lowest FWHM value in each case allows one to estimate the linewidth limited by homogeneous broadening. Any motional process that yields a simulated linewidth lower than the experimental homogenous broadening cannot be extracted from the data.

MAPbI_3 (3 kHz MAS)		**FA**PbI_3 (3 kHz MAS)		**$FA_{0.67}MA_{0.33}PbI_3$** (20 kHz MAS)		
T [K]	FWHM [Hz]	T [K]	FWHM [Hz]	T [K]	FWHM (FA) [Hz]	FWHM (MA) [Hz]
326	**26**	333	**45**	333 K	**60-65**	**20-24**
323	27	324	59			
320	27	294	73			
310	34	288	79			
300	61	281	115			
		267	115			
		240	270			

Details of DFT calculations of EFG tensors

EFG parameters

$FACs_{19}Pb_8I_{36}$ (cubic)

1) **Vzz =** -0.612695 a.u., **NQCC** = -2.94258 MHz, **asym. parameter η** = 0.68865
2) **Vzz** = -0.557585 a.u., **NQCC** = -2.67790 MHz, **asym. parameter η** = 0.71117

$MACs_{19}Pb_8I_{36}$ (tetragonal)

Vzz = 0.160433 a.u., **NQCC** = 0.770507 MHz, **asym. parameter η** = 0.18422

Cluster generation

The crystal structures of cubic (black) $FAPbI_3$[7] and tetragonal (black) $MAPbI_3$[8] were used as a starting point for the clusters. In a first step the proton positions in the periodic system were density functional theory (DFT) optimized using the generalized gradient approximation (GGA) functional PBE[9] including relativistic effects (with spin-orbit coupling) and the Grimme[10] dispersion correction within the Quantum Espresso suite[11]. In every calculation a plane-wave maximum cutoff energy of 90 Ry and a 3x3x3 Monkhorst-Pack[12] grid of k-points was employed.

The final clusters were assembled from the relaxed structures as a central MA^+/FA^+ ion enclosed by a Pb-I cage including 19 surrounding MA^+/FA^+ to ensure charge compensation[13]. The surrounding MA^+/FA^+ ions were then replaced by Cs^+ ions, leading to a cubic $FACs_{19}Pb_8I_{36}$ and a tetragonal $MACs_{19}Pb_8I_{36}$ cluster.

EFG tensor calculation

The EFG tensor calculations were performed at DFT level using the GGA BP86[14-15] functional including relativistic effects (with spin-orbit coupling) with the ZORA[16-18] approximation and the Grimme[10] dispersion correction implemented within the Amsterdam Density Functional (ADF)[19-20] suite.All-electron basis sets were used, which were triple-ζ in the valence with two polarization functions (TZ2P)[21]. Both the cluster generation and the EFG tensor calculations were parametrized according to recent studies on calculations of electronic and magnetic properties of heavy atoms.[13, 22-25]

References

1. Knop, O.; Wasylishen, R. E.; White, M. A.; Cameron, T. S.; Vanoort, M. J. M., *Can. J. Chem.* **1990,** *68* (3), 412-422.
2. Roiland, C.; Trippe-Allard, G.; Jemli, K.; Alonso, B.; Ameline, J. C.; Gautier, R.; Bataille, T.; Le Polles, L.; Deleporte, E.; Even, J.; Katan, C., *PCCP* **2016,** *18* (39), 27133-27142.
3. Gong, J.; Yang, M. J.; Ma, X. C.; Schaller, R. D.; Liu, G.; Kong, L. P.; Yang, Y.; Beard, M. C.; Lesslie, M.; Dai, Y.; Huang, B. B.; Zhu, K.; Xu, T., *J. Phys. Chem. Lett.* **2016,** *7* (15), 2879-2887.
4. Rosales, B. A.; Men, L.; Cady, S. D.; Hanrahan, M. P.; Rossini, A. J.; Vela, J., *Chem. Mater.* **2016,** *28* (19), 6848-6859.
5. Rosales, B. A.; Hanrahan, M. P.; Boote, B. W.; Rossini, A. J.; Smith, E. A.; Vela, J., *ACS Energy Lett.* **2017,** *2*, 906-914.
6. Shmyreva, A. A.; Safdari, M.; Furo, I.; Dvinskikh, S. V., *J. Chem. Phys.* **2016,** *144* (22), 224201-224206.
7. Weller, M. T.; Weber, O. J.; Frost, J. M.; Walsh, A., *J. Phys. Chem. Lett.* **2015,** *6* (16), 3209-3212.
8. Weber, D., *Zeitschrift Fur Naturforschung Section B-a Journal of Chemical Sciences* **1978,** *33* (12), 1443-1445.
9. Perdew, J. P.; Burke, K.; Ernzerhof, M., *Phys. Rev. Lett.* **1997,** *78* (7), 1396-1396.
10. Grimme, S., *J. Comput. Chem.* **2006,** *27* (15), 1787-1799.
11. Giannozzi, P.; Baroni, S.; Bonini, N.; Calandra, M.; Car, R.; Cavazzoni, C.; Ceresoli, D.; Chiarotti, G. L.; Cococcioni, M.; Dabo, I.; Dal Corso, A.; de Gironcoli, S.; Fabris, S.; Fratesi, G.; Gebauer, R.; Gerstmann, U.; Gougoussis, C.; Kokalj, A.; Lazzeri, M.; Martin-Samos, L.; Marzari, N.; Mauri, F.; Mazzarello, R.; Paolini, S.; Pasquarello, A.; Paulatto, L.; Sbraccia, C.; Scandolo, S.; Sclauzero, G.; Seitsonen, A. P.; Smogunov, A.; Umari, P.; Wentzcovitch, R. M., *Journal of Physics-Condensed Matter* **2009,** *21* (39).
12. Pack, J. D.; Monkhorst, H. J., *Physical Review B* **1977,** *16* (4), 1748-1749.
13. Giorgi, G.; Yoshihara, T.; Yamashita, K., *PCCP* **2016,** *18* (39), 27124-27132.
14. Perdew, J. P., *Physical Review B* **1986,** *33* (12), 8822-8824.
15. Becke, A. D., *Physical Review A* **1988,** *38* (6), 3098-3100.
16. Vanlenthe, E.; Baerends, E. J.; Snijders, J. G., *J. Chem. Phys.* **1994,** *101* (11), 9783-9792.
17. Vanlenthe, E.; Baerends, E. J.; Snijders, J. G., *J. Chem. Phys.* **1993,** *99* (6), 4597-4610.
18. van Lenthe, E.; Ehlers, A.; Baerends, E. J., *J. Chem. Phys.* **1999,** *110* (18), 8943-8953.
19. Guerra, C. F.; Snijders, J. G.; te Velde, G.; Baerends, E. J., *Theor. Chem. Acc.* **1998,** *99* (6), 391-403.
20. te Velde, G.; Bickelhaupt, F. M.; Baerends, E. J.; Guerra, C. F.; Van Gisbergen, S. J. A.; Snijders, J. G.; Ziegler, T., *J. Comput. Chem.* **2001,** *22* (9), 931-967.
21. Van Lenthe, E.; Baerends, E. J., *J. Comput. Chem.* **2003,** *24* (9), 1142-1156.
22. Alkan, F.; Dybowski, C., *J. Phys. Chem. A* **2016,** *120* (1), 161-168.
23. Dmitrenko, O.; Bai, S.; Beckmann, P. A.; van Bramer, S.; Vega, A. J.; Dybowski, C., *J. Phys. Chem. A* **2008,** *112* (14), 3046-3052.
24. Even, J.; Pedesseau, L.; Jancu, J. M.; Katan, C., *J. Phys. Chem. Lett.* **2013,** *4* (17), 2999-3005.
25. Alkan, F.; Dybowski, C., *PCCP* **2014,** *16* (27), 14298-14308.